# Taste breaking in the minimally doubled Karsten-Wilczek action and its tree-level improvement

S. Borsányi,[1] S. Capitani,[1] Z. Fodor,[2,1,3,4] D. Godzieba,[2] P. Parotto,[5] R. A. Vig,[1] and C. H. Wong[1]

[1]*University of Wuppertal, Department of Physics, Wuppertal D-42119, Germany*
[2]*Pennsylvania State University, Department of Physics, State College, Pennsylvania 16801, USA*
[3]*Institute for Theoretical Physics, ELTE Eötvös Loránd University, Pázmány P. sétány 1/A, H-1117 Budapest, Hungary*
[4]*Jülich Supercomputing Centre, Forschungszentrum Jülich, D-52425 Jülich, Germany*
[5]*Dipartimento di Fisica, Università di Torino and INFN Torino, Via P. Giuria 1, I-10125 Torino, Italy*

(Received 17 February 2025; accepted 19 March 2025; published 15 April 2025)

Minimally doubled fermion actions offer a discretization for two-flavor quantum chromodynamics without rooting, but retaining a U(1) chiral symmetry at the same time. The price to pay is a breaking of the hypercubic symmetry, which requires the inclusion and tuning of new counterterms. Similar to staggered quarks, these actions suffer from taste breaking. We perform a mixed-action numerical study with the Karsten-Wilczek formulation of minimally doubled fermions on 4stout staggered configurations, generated with physical quark masses, covering a broad range of lattice spacings. We consider a tree-level spatial Naik improvement to mitigate discretization errors. We carry out a nonperturbative tuning of the KW action with and without improvement and investigate the taste breaking and the approach to the continuum limit.

DOI: 10.1103/PhysRevD.111.074510

## I. INTRODUCTION

Dynamical lattice simulations use a variety of discretizations of the quantum chromodynamics (QCD) action, which differ by the features they conserve from the continuum theory, ease of implementation and numerical cost. Perhaps the most widespread formulation is the Wilson action where an additional clover term is introduced to ensure that the errors come $\mathcal{O}(a^2)$ of the lattice spacing [1]. This action has been used in several precision studies in the recent past to calculate $n$-point functions in the QCD vacuum, e.g. hadron spectroscopy [2]. On the other hand, when studying the chiral transition of finite temperature QCD, and in particular the phase diagram of the theory, actions which preserve a remnant chiral symmetry are preferable, if not mandatory. Since chiral actions are in general numerically expensive, we owe the vast majority of QCD thermodynamics results in the literature to their cheapest version, namely staggered quarks [3]. Because the staggered discretization suffers from fourfold doubling for each flavor of fermion, rooting is required on the quark determinant whenever the number of degenerate fermion flavors is not a multiple of four. The soundness of fermion rooting has been debated for a long time [4–7]. At the very least, rooting gives a well-defined procedure at vanishing chemical potential, where the fermion determinant is real. This is not the case, however, when a (real) chemical potential is introduced, and the determinant becomes complex.

Among the most common methods to circumvent the complex action problem of QCD at real chemical potential are reweighting techniques [8–15], which have enjoyed promising developments in recent years [16–19]. In the case of $N_f = 2$ degenerate light flavors, the rooting at finite chemical potential suffers from a sign ambiguity. It was shown in Ref. [20] that staggered rooting at finite chemical potential leads to unphysical effects in the thermodynamics at low temperatures, as a remnant of pion condensation at finite isospin chemical potential.

In order to avoid the rooting of the light quarks, one possibility is to employ so-called minimally doubled fermions. As the name suggests, minimally doubled fermions have the minimum number of doublers allowed by the Nielsen-Ninoyima no-go theorem [21] while still maintaining a remnant chiral symmetry with a strictly local Dirac operator. Minimally doubled fermions reduce the number of doublers from 15 to one, leaving two degenerate mass species. In the vast majority of thermodynamics studies, up and down quarks are treated as degenerate. Hence in the $N_f = 2$ theory the number of quark states is the correct one, and no rooting procedure is necessary. In the case of the $N_f = 2 + 1$ theory, a rooting of the strange quark determinant would still be necessary. However, the unphysical effects of rooting in this case would appear at rather large strange chemical potentials, in a regime which is beyond the reach of current reweighting methods. The remnant chiral symmetry is a feature that makes minimally doubled fermions particularly attractive for thermodynamics studies. The major drawback is that the resulting breaking of hypercubic symmetry requires the introduction of counterterms that have no counterpart in the continuum theory. This makes the renormalization process more involved than with other actions. The most popular versions of minimally doubled fermion actions are the Karsten-Wilczek (KW) [22,23] and Boriçi-Creutz (BC) [24,25] fermions, although other types exist, including generalizations of both [26–28].

The most relevant concern about minimally doubled fermions comes from the apparent $\mathcal{O}(a)$ discretization errors. The origin of this effect is the inclusion of a dimension-five term, a 3D Laplacian operator, designed to eliminate the spatial doublers. This has the consequence that both the self-energy and the vacuum polarization diagrams suffer from terms that are odd in $a$, similarly to the unimproved Wilson action. It is natural to expect that an improvement program can be introduced based on the distinct dimension-five operators of the theory [29]. However, even in its unimproved form, the action has an automatic improvement feature for some applications: precisely the terms that are odd in the lattice spacing are also odd in one of the broken symmetries (e.g. charge conjugation or time reversal) [30]. If that symmetry is restored on the level of the observable, such terms will cancel, as long as the gauge configurations are generated with an action that respects the discrete symmetries. This is a typical pattern in mixed-action studies like the present one.

For dynamical minimally doubled fermions we know from perturbation theory that terms which are effectively of order $a$ appear as leading logarithms $ag_0^{2n}\log^n a$ in the loop amplitudes, where $g_0$ is the bare gauge coupling, running with the lattice spacing as $g_0^2 \sim 1/\log a$. As a first step toward full improvement we introduce a tree-level improved action, which has the effect of eliminating the leading logarithms, so that the amplitudes behave as $ag_0^{2n}\log^{n-1} a$ [31]. At one loop this means that the leading logarithms $ag_0^2\log a$ disappear, leaving finite $\sim ag_0^2$ terms as leading corrections.

In this work we use a Naik-type (three-hop) construction to achieve tree-level improvement. The new irrelevant term is designed to raise the dimensionality of the 3D Laplacian, at least on a trivial gauge background. We will show in a separate publication that this type of improvement eliminates the leading log divergences [32].

Though in a mixed-action study odd terms in $a$ cancel on average for $C$ or $T$ symmetric observables, the symmetry-breaking terms increase the statistical errors. The decrease of magnitude of the radiative corrections from $ag_0^2\log a$ to $ag_0^2$ thanks to improvement has the consequence of reducing the statistical noise in the functional integral which is sampled in Monte Carlo simulations, as we can see in our calculation of the pion decay constant $f_\pi$.

In this work we present a study of the tuning procedure and the taste breaking of the Karsten-Wilczek action. We do so on a gauge background generated with the 4stout action, employing a tree-level Symanzik gauge action and a staggered fermionic action with four levels of stout smearing. We implement both the original unimproved version of the KW action as well as a tree-level Naik improved version, discussed in Secs. II and III, respectively. In both cases we carry out the nonperturbative renormalization (Sec. IV) and test the consistency of the continuum result for the pion decay constant with the staggered formulation (Sec. V). Finally, we determine the taste-breaking features of the action in both scenarios (Sec. VI) and discuss the corresponding computational demands in Sec. VII.

## II. THE KARSTEN-WILCZEK ACTION

The first and simplest formulation of minimally doubled fermions is due to Karsten [22] and Wilczek [23], whereby the single remaining doubler lies on one of the axes of the Brillouin zone. Like Wilson fermions this is achieved by adding a term to the naïve action that is proportional to a Laplacian. Minimally doubled fermions have the extra requirement to anticommute with $\gamma_5$, in order not to violate chiral symmetry. Thus, the Laplacian term cannot be added in all directions. At most a 3D Laplacian can be considered, multiplied by the $\gamma$ matrix of the fourth direction. This construction leaves only one doubler lying in the fourth space-time direction in the Brillouin zone. This design inherently breaks the hypercubic symmetry of the lattice down to a cubic symmetry corresponding to the doubler-free directions. Wilczek generalized the action by introducing the so-called Wilczek parameter $\zeta$.

The tree-level Karsten-Wilczek action is given by

$$S_F^{\mathrm{KW}} = S_F^N + \sum_x \bar{\psi}(x)\frac{i\zeta}{2}\gamma_\alpha \sum_{\mu\neq\alpha}(2\psi(x) - U_\mu(x)\psi(x+\hat{\mu}) - U_\mu^\dagger(x-\hat{\mu})\psi(x-\hat{\mu})), \tag{1}$$

where $S_F^N$ is the naïve fermion action

$$S_F^N = \sum_x\sum_\mu \bar{\psi}(x)\gamma_\mu\frac{1}{2}[U_\mu(x)\psi(x+\hat{\mu}) - U_\mu^+(x-\hat{\mu})\psi(x-\hat{\mu})] + m\sum_x\bar{\psi}(x)\psi(x). \tag{2}$$

Here, $U_\mu(x)$ are the links in direction $\mu$ at lattice site $x$. The sum over the directions $\mu\neq\alpha$ implements a three-dimensional covariant Laplacian. This is the so-called Karsten-Wilczek term and is analogous to a Wilson term though with a different gamma matrix structure. The action is minimally doubled if its coefficient, the Karsten-Wilczek parameter, obeys $|\zeta| > 1/2$. The different treatment of direction $\alpha$ and the three other directions introduces an anisotropy. It is convenient to choose $\alpha$ as the temporal direction.

While the action at first sight looks more similar to Wilson fermions, due to an exact remnant chiral symmetry, the spectrum of the massless Dirac operator is on the imaginary line, similarly to naïve and staggered fermions. Karsten-Wilczek fermions also perceive the global topological charge the same way as naïve and staggered fermions do [33,34].

The breaking of the hypercubic symmetry causes the appearance of relevant and marginal operators which are not present in the continuum theory and, thus, requires the addition of counterterms. It was shown in Ref. [35] that there is a single relevant operator of dimension 3 appearing, the Lorentz-symmetry-breaking term $i\bar{\psi}\gamma_\alpha\psi$. It was shown in Ref. [36] that such a term cannot be avoided in chirally symmetric, minimally doubled actions. Additionally, the dimension 4 counterterm $\bar{\psi}\gamma_\alpha D_\alpha\psi$ amounting to a renormalization of the fermionic speed of light appears [35–37]. Because of quark-gluon interactions, the breaking of hypercubic symmetry propagates to the gauge sector and requires the presence of a gluonic counterterm $\sum_{\mu\neq\alpha} F^2_{\alpha\mu}$, of dimension 4, which amounts to a renormalization of the gluonic speed of light [35–37].

The two fermionic counterterms (of dimensions 3 and 4) and one gluonic counterterm (of dimension 4) can be defined on the lattice as

$$\begin{aligned} S^{3f} &= c\sum_x \bar{\psi}(x) i\gamma_\alpha\psi(x), \\ S^{4f} &= (\xi_0 - 1)\sum_x \bar{\psi}(x)\frac{1}{2}\gamma_\alpha(U_\alpha(x)\psi(x+\hat{\alpha}) \\ &\quad - U^\dagger_\alpha(x-\hat{\alpha})\psi(x-\hat{\alpha})), \\ S^{4g} &= d_G\sum_x\sum_{\mu\neq\alpha} \mathrm{Re}\,\mathrm{Tr}(1-\mathcal{P}_{\mu\alpha}(x)), \end{aligned} \tag{3}$$

where $\mathcal{P}_{\mu\alpha}(x)$ are the plaquettes on the $\mu$–$\alpha$ plane at lattice site $x$. Throughout this work, we identify the direction $\alpha$ with the temporal direction $\alpha = 0$. The nonperturbative tuning of the parameters $c$, $\xi_0$ and $d_G$ using mesonic correlation functions was demonstrated in quenched QCD in Ref. [29].

The Dirac operator reads

$$\begin{aligned} D_{\mathrm{KW}}\psi(x) \equiv \frac{1}{2}\sum_\mu &[c_\mu(x)\Gamma_\mu U_\mu(x)\psi(x+\hat{\mu}) \\ &- c_\mu^{-1}(x-\hat{\mu})\Gamma^\dagger_\mu U^\dagger_\mu(x-\hat{\mu})\psi(x-\hat{\mu})] \\ &+ (m + i(3\zeta + c)\gamma_0)\psi(x), \end{aligned} \tag{4}$$

where

$$\Gamma_\mu = \begin{cases} \gamma_\mu - i\zeta\gamma_0 & \mu\neq 0, \\ \xi_0\gamma_\mu & \mu = 0, \end{cases} \tag{5}$$

and the boundary conditions, together with a (in general complex) chemical potential $\mu_q$, are encoded in

$$c_\mu(x) = e^{\frac{\mu_q}{N_t}\delta_{0\mu}}\Phi(x), \tag{6}$$

and $\Phi(x) = \pm 1$.

The unimproved action has been subject to a detailed discussion in the Ph.D. thesis of Weber [30]. It was pointed out that the Karsten-Wilczek term in the action is odd both with respect to charge conjugation and to the reversal of the $\alpha$ direction, but even for the product of the two. This term is the only source of $\mathcal{O}(a)$ errors. The sign of the symmetry-breaking contributions can, in principle, be flipped if $\zeta$ is turned from $+1$ to $-1$. This feature can, under some circumstances, be exploited to cancel the $\mathcal{O}(a)$ effects. In the next section we will follow the idea of Hamber and Wu [38] and address the dimensionality of the Karsten-Wilczek term.

## III. NAIK IMPROVEMENT

In order to reduce discretization errors and facilitate the extrapolation to the continuum, in this work we explore the introduction of additional terms to improve the action. A simple choice is the Naik improvement [39], which we apply in the three spatial directions to address the discretization errors coming from the Karsten-Wilczek term. The Naik term, which is part of the highly improved staggered quarks (HISQ) action, is often used to improve the $\mathcal{O}(a^2)$ errors of the Nabla operator [40].

In this work we do not intend to reduce $\mathcal{O}(a^2)$ errors. We also foresee the application of the Karsten-Wilczek actions in a thermodynamic context and shall maintain the possibility to apply the reduced matrix formalism. In that formalism multihop terms in Euclidean time are very difficult to accommodate, but a more sophisticated spatial structure is not an issue. Thus, we apply the three-hop term in space only. Because the action is anisotropic by construction, the lack of improvement in the temporal direction might be compensated by a smaller temporal lattice spacing, i.e., a renormalized anisotropy $\xi_f = a_s/a_t > 1$, a possibility that we leave for future work.

In momentum space, like in the Wilson action, the correlator of the KW Dirac operator consists of a Nabla and a Laplacian. The unimproved inverse propagator reads

$$D_{\mathrm{KW}}(k) = \frac{i}{a}\left[\sum_{\mu=0}^{3}\gamma_\mu\xi_\mu\sin ak_\mu + \zeta\gamma_0\sum_{\mu=1}^{3}(1-\cos ak_\mu)\right], \tag{7}$$

where

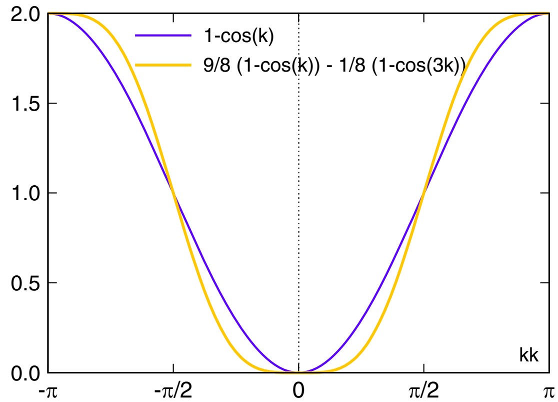


FIG. 1. The Laplacian term and its three-hop improved form in momentum space in one of the spatial directions. The improved operator is proportional to $\sim k^4$ instead of the original $\sim k^2$ form.

$$\xi_\mu = \begin{cases} 1 & \mu \neq 0, \\ \xi_0 & \mu = 0, \end{cases} \tag{8}$$

the $\sin ak_\mu$ term represents the single-hop Nabla, and the $(1 - \cos ak_\mu)$ is a Laplacian term in direction $\mu$.

We improve the Dirac operator with extra hop terms with an odd number of steps so that we do not spoil the even-odd preconditioning. The cheapest option seems to be the Naik improvement with linear triple hops in each spatial direction. The improvement of the Nabla is straightforward:

$$\begin{aligned} \nabla^{\mathrm{NAIK}}\Psi &= \frac{i}{a}[s_1 \sin ak_j + s_3 \sin 3ak_j]\Psi(k) \\ &= i[k_j + 0k_j^3 + \mathcal{O}(k^5)], \end{aligned} \tag{9}$$

where the requirement in the last equality is satisfied with the choice $s_1 = 9/8$, $s_3 = -1/24$.

With the improvement of the Laplacian the goal is to suppress the momentum dependence of the cosine term altogether, simultaneously lifting the momenta in the doubler's part of the Brillouin zone. In momentum space we can eliminate the $\mathcal{O}(k^2)$ term in the expression

$$(1-\cos ak_j) \to c_1(1-\cos ak_j) + c_3(1-\cos 3ak_j) \tag{10}$$

with the choice $c_1 = 9/8$, $c_3 = -1/8$.

The resulting Laplacian operator in one spatial direction, in momentum space, is shown in Fig. 1. We can appreciate how the improvement of the Laplacian reduces the momentum dependence around $k = 0$ and at the same time lifts the momenta in the vicinity of the edges of the Brillouin zone, as desired.

The full 3D Naik-improved Dirac operator reads

$$\begin{aligned} D^{\mathrm{NAIK}}\psi(x) \equiv \frac{1}{2}\sum_\mu &[c_\mu(x)\Gamma_\mu^{(1)}U_\mu(x)\psi(x+\hat{\mu}) - c_\mu^{-1}(x-\hat{\mu})\Gamma_\mu^{(1)\dagger}U_\mu^\dagger(x-\hat{\mu})\psi(x-\hat{\mu}) \\ &+ c_\mu(x)c_\mu(x+\hat{\mu})c_\mu(x+2\hat{\mu})\Gamma_\mu^{(3)}U_\mu(x)U_\mu(x+\hat{\mu})U_\mu(x+2\hat{\mu})\psi(x+3\hat{\mu}) \\ &- c_\mu^{-1}(x-\hat{\mu})c_\mu^{-1}(x-2\hat{\mu})c_\mu^{-1}(x-3\hat{\mu})\Gamma_\mu^{(3)\dagger}U_\mu^\dagger(x-\hat{\mu})U_\mu^\dagger(x-2\hat{\mu})U_\mu^\dagger(x-3\hat{\mu})\psi(x-3\hat{\mu})] \\ &+ (m + i(3\zeta + c)\gamma_0)\psi(x), \end{aligned} \tag{11}$$

where we used the new notations:

$$\Gamma_\mu^{(1)} = \begin{cases} \bar{s}_1\gamma_\mu - i\bar{c}_1\gamma_0 & \mu \neq 0, \\ \xi_0\gamma_0 & \mu = 0, \end{cases} \tag{12}$$

$$\Gamma_\mu^{(3)} = \begin{cases} \bar{s}_3\gamma_\mu - i\bar{c}_3\gamma_0 & \mu \neq 0, \\ 0 & \mu = 0, \end{cases} \tag{13}$$

and the additional parameters satisfy

$$1 = \bar{s}_1 + 3\bar{s}_3, \tag{14}$$

$$\zeta = \bar{c}_1 + \bar{c}_3. \tag{15}$$

In the improved Laplacian we have

$$\bar{c}_1 = \zeta\frac{9}{8} \quad \text{and} \quad \bar{c}_3 = -\zeta\frac{1}{8}, \tag{16}$$

and in the improved Nabla operator we need

$$\bar{s}_1 = \frac{9}{8} \quad \text{and} \quad \bar{s}_3 = -\frac{1}{24}. \tag{17}$$

In general, with the new gamma matrix structure the half-vector trick cannot be used. However, it becomes applicable if $\Gamma^j \sim \gamma^j \mp i\gamma^0$. Hence, one may sacrifice the exact Naik (spatial) tree-level improvement to utilize the half-vector trick. We note that this is not a complete tree-level improvement, as the temporal direction remains unimproved. In fact, the main goal of this improvement program is to minimize the lattice artifacts brought in by the $a\zeta\gamma^0\triangle$ operator, through replacing the Laplacian by a higher-order derivative, while the improvement of the spatial Nabla is of secondary importance. Thus, we have the freedom to fix $\bar{s}_1$, $\bar{s}_3$ and $\zeta$ to maintain $\bar{s}_1 = \bar{c}_1$ and $\bar{s}_3 = \bar{c}_3$, while also keeping $\bar{c}_1 = \zeta 9/8$ and $\bar{c}_3 = -\zeta/8$.

This can be achieved with the choice

$$\bar{s}_1 = \bar{c}_1 = 1.5,$$
$$\bar{s}_3 = \bar{c}_3 = -1/6,$$
$$\zeta = 4/3. \tag{18}$$

This is the choice we employ in this work. The case of no improvement means $\bar{c}_3 = \bar{s}_3 = 0$, which requires $c_1 = 1$, so $\bar{c}_1 = \zeta$ and $s_1 = \bar{s}_1 = 1$. This admits the half-vector trick if and only if $\zeta = \pm 1$.

## IV. NONPERTURBATIVE RENORMALIZATION

### A. Lattice details

This is a mixed-action study. We use five gauge ensembles that were generated using the 4stout staggered action with tree-level Symanzik improvement in the gauge sector [41]. The ensembles were generated along the line of constant physics with $2+1+1$ flavors, where the pion and kaon masses were tuned to assume the physical ratios to $f_\pi$. The ensembles in this work are listed in Table I.

Throughout this work we employ the $w_0$-based scale setting with $w_0 = 0.17236$ fm, as of Ref. [42]. All masses, expressed in MeV, are based on this $w_0$ scale obtained on the 4stout-staggered gauge configurations.

We implemented the Karsten-Wilczek Dirac operator both for the standard and the three-hop setup. Having avoided a two-hop form for the improvement we could benefit from even-odd preconditioning [43]. We note that, being chiral, the Karsten-Wilczek operator turns an $L$-handed Weyl spinor into an $R$-handed spinor and vice versa. This allows one to formulate a solver for the $L$ spinor, with the benefit of working with a half-sized spinor. This trick is the analogous of the even-odd decomposition of the staggered operator.

The solver, which is based on the $L/R$ decomposition, is outperformed by the even-odd preconditioned solver, because the latter works with an effective operator with reduced condition number. Indeed, the Karsten-Wilczek operator lends itself to such preconditioning:

$$\begin{pmatrix} M_{ee} & M_{eo} \\ M_{oe} & M_{oo} \end{pmatrix} \begin{pmatrix} \phi_e \\ \phi_o \end{pmatrix} = \begin{pmatrix} \eta_e \\ \eta_o \end{pmatrix} \tag{19}$$

TABLE I. The staggered ensembles and the bare parameters of the 4stout action. The charm mass is always $m_c = 11.85 m_s$. Each ensemble is 144 configurations strong.

| $\beta$ | $a$ [fm] | $N_x \times N_\tau$ | $m_{ud}$ | $m_s$ |
|---|---|---|---|---|
| 3.6376 | 0.1581 | $40 \times 64$ | 0.00243956 | 0.0687299 |
| 3.7089 | 0.1308 | $48 \times 64$ | 0.00201959 | 0.0566136 |
| 3.7589 | 0.1152 | $64 \times 96$ | 0.00178099 | 0.0496697 |
| 3.8360 | 0.0953 | $64 \times 96$ | 0.00147176 | 0.0407946 |
| 4.0126 | 0.0638 | $96 \times 144$ | 0.000958973 | 0.0264999 |

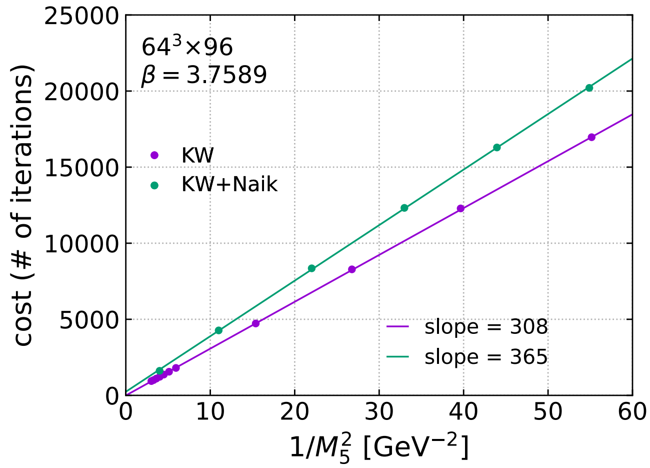


FIG. 2. Number of iterations vs the pion mass. The improved action has a slightly higher condition number.

for some source $\eta$ and solution $\phi$. A key feature of the Karsten-Wilczek operator is that $M_{ee}$ and $M_{oo}$ are strictly local. One can express $\phi_o$ in terms of $\phi_e$:

$$\phi_o = M_{oo}^{-1}(\eta_o - M_{oe}\phi_e).$$

Therefore one can solve for $\phi_e$ alone:

$$(M_{ee} - M_{eo}M_{oo}^{-1}M_{oe})\phi_e \equiv \hat{M}\phi_e = \eta_e - M_{eo}M_{oo}^{-1}\eta_o$$

in which $\hat{M}$ is even-even only. $\gamma_5\hat{M}$ is Hermitian, though not positive. This is in contrast with the $L/R$ decomposed solver where the product $M_{LR}M_{RL}$ is Hermitian and positive; thus, a conjugate gradient algorithm is applicable. Luckily the conjugate residual algorithm (see e.g. Ref. [44]) performs well for $\gamma_5\hat{M}$. The so-called "half-vector trick," that relies on the projector nature of the gamma matrix structure of the nonlocal terms, is an independent optimization we adopted. In total, the three-hop operators arithmetic weight is roughly double that of the Wilson action. We plot the iteration count as a function of the pseudoscalar mass for one of our ensembles in Fig. 2.

### B. Tuning

In this section we illustrate the procedure we employed to tune the parameters of the KW action. We need to carry out a multidimensional tuning involving the KW parameters $c$ and $\xi_0$, as well as the fermion mass $m_0$. The KW parameter $d_G$ is not tuned, as the gauge configurations were generated with our 4stout staggered action. We will show in the following that the tuning largely decouples, and the three parameters $c$, $\xi_0$ and $m_0$ can be tuned one at a time.

#### 1. Tuning the dimension-three counterterm

As shown in Ref. [29], in order to tune $c$ it is convenient to exploit the existence of oscillating contributions, related to fermion doubling [30], to the correlation functions in the direction $\alpha$ of certain meson interpolating operators

$$C_\Gamma(n-m) \sim \langle \bar{\psi}(n)\Gamma\psi(n)\bar{\psi}(m)\Gamma\psi(m)\rangle. \tag{20}$$

Crucially, the frequency of these oscillations is very sensitive to the value of $c$.

Fermion parity partners can be identified by the spin-taste structure of the KW action, which was thoroughly discussed in Refs. [45,46]. For pseudoscalar mesons, two relevant tastes are the $\gamma_0$ (since $\alpha = 0$ in this work) and $\gamma_5$ channels, where the latter can be identified with the physical pion. The correlators for $\gamma_0$ and $\gamma_5$ are taken *parallel* to the preferred axis of the KW action, $\alpha = 0$ in this case. The parallel correlator for $\gamma_0$ exhibits oscillations while that of $\gamma_5$ does not. The tuning criterion for the $c$ parameter is where the frequency spectrum of the oscillations of the $\gamma_0$ channel recovers its tree-level form [30]. At the tuned $c$, the oscillation of the $\gamma_0$ correlator is described by $(-1)^n$, where $n$ is the temporal separation of source and sink. The frequency of the oscillation at a given $c$ value can be described by $\omega = \omega_c + \pi$, where $\pi$ is the frequency of the rapid oscillations at tuned $c$ given by the $(-1)^n$ factor and $\omega_c$ is a beat frequency that appears in the rapid oscillations when $c$ is detuned. Thus, the tuning criterion can be equivalently stated as where $\omega_c = 0$ and the beat vanishes [30]. Figure 3 shows an example of correlators in the $\gamma_0$ and $\gamma_5$ channels at detuned $c$, where both the rapid oscillation and the beat oscillation can be observed for $\gamma_0$.

We average over the symmetric halves of the $\gamma_0$ correlator $C_0(n)$ and eliminate the rapid oscillation with a factor of $(-1)^n$:

$$C(n) = (-1)^n \frac{1}{2}(C_0(n) + C_0(N_t - n)), \tag{21}$$

for $0 \leq n \leq N_t/2$, where $N_t$ is the temporal extent of the lattice. Then, the correlator is well described by the model

$$C(n) \approx A\cosh(M(n - N_t/2))\cos(\omega_c n - \phi), \tag{22}$$

where $M$ is the mass of $\gamma_0$ in lattice units and $\phi$ is a phase factor, and one can see that the beat frequency and the mass decouple.

An immediate difficulty that arises in tuning $c$ is due to the finite length of the lattice, which makes fitting the frequency unreliable when the wavelength of the beat is greater than $N_t$, in the relative vicinity of tuned $c$. This can be ameliorated through the use of tiling gauge configurations. Tiling means the gauge configurations are concatenated in the desired direction (time in our case) to form $N_x^3 \times (2N_t)$ or $N_x^3 \times (4N_t)$ lattices on which the propagator is measured. The top panel of Fig. 4 shows an example of $C(n)$ at detuned $c$ for 1× (i.e., no tiling), 2× and 4× tiling. This allows one to study the propagator in a longer range than that of the dynamical simulation. Tiling extends the

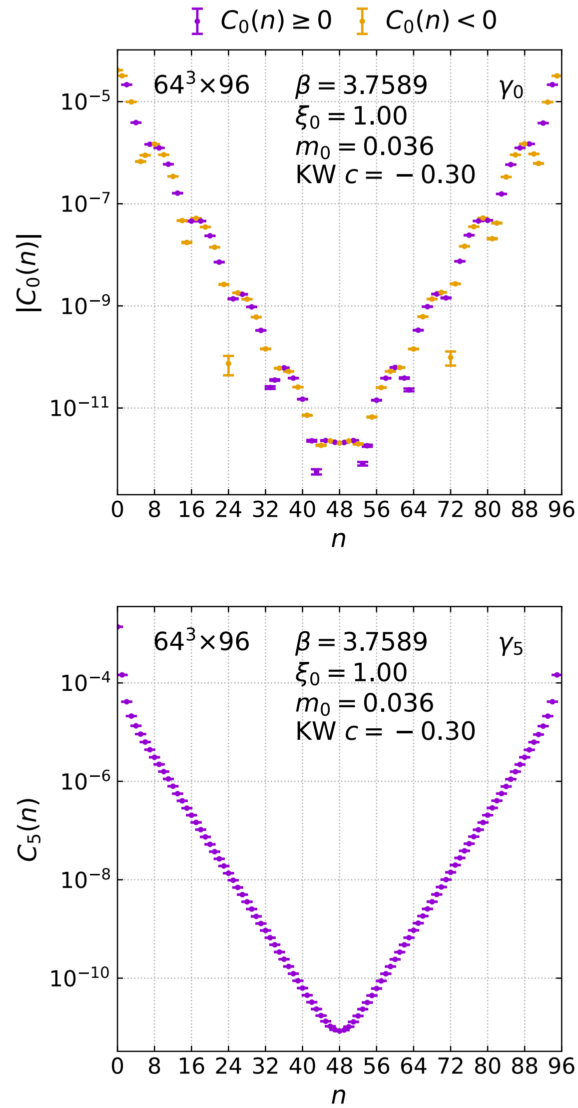


FIG. 3. Correlators for the $\gamma_0$ (top) and $\gamma_5$ (bottom) fermion channels for the Karsten-Wilczek action. The frequency of the oscillating $\gamma_0$ correlator depends on the $c$ parameter of the action. A beat oscillation on top of the $(-1)^n$ oscillation (visible in the top plot) occurs when the $c$ parameter is detuned.

idea of a mixed-action study where the quarks live on an extended lattice without maintaining the long wavelength gauge fluctuations, which would anyway be irrelevant for the divergent parts of the Feynman diagrams. Thus, when used properly, tiling the stored gauge configurations increases the precision with which $\omega_c$ is measured. This is evident from the bottom panel of Fig. 4, where the measured beat frequency $\omega_c(c)$ is shown for each level of tiling. We use 4× and occasionally 1× tiling throughout this study.

Regardless of tiling, $c$ is tuned for a given pair $\xi_0$, $m_0$ by scanning through $c$ and searching for $\omega_c(c) = 0$. As shown already in Ref. [29], the behavior of $\omega_c(c)$ is basically linear on both sides of the tuned value of $c$. An example of

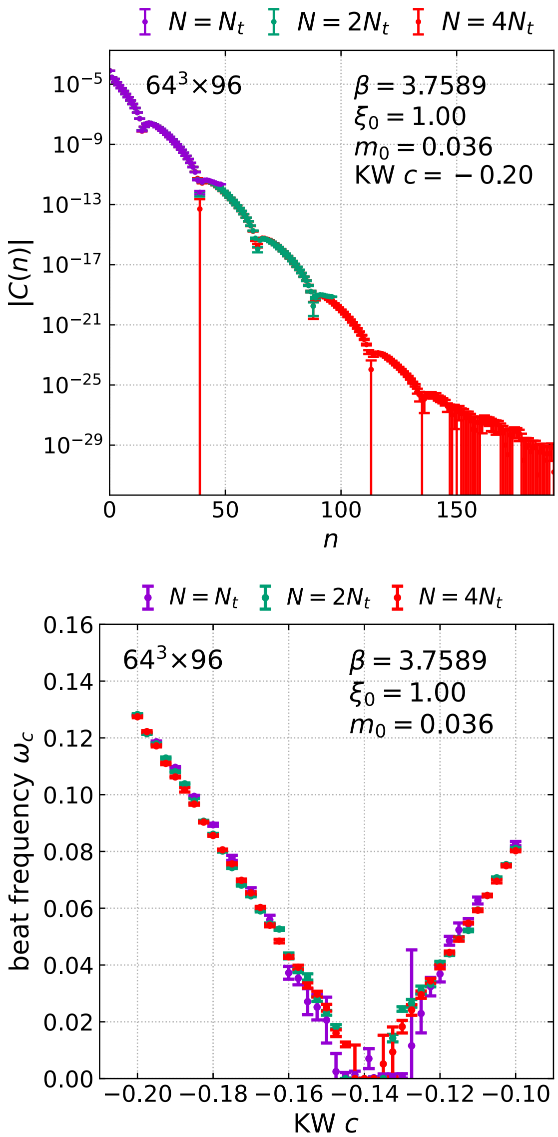


FIG. 4. Top: the symmetrized $\gamma_0$ correlator measured with different amounts of tiling with stored gauge configurations. The proper use of tiling permits longer correlation lengths to be measured and increases the precision of the measurement of the beat frequency $\omega_c$. Bottom: measurements of $\omega_c$ as a function of the $c$ parameter at the same three tilings.

this is shown in Fig. 5, where the final result is obtained by combining linear fits on either side of the tuned $c$. Throughout this work, we find that linear fits to both sides were unproblematic and yielded consistently good $p$ values.

#### 2. *Tuning the bare anisotropy $\xi_0$*

The physical anisotropy can be determined using a $\gamma_5$ correlator in a direction perpendicular to $\alpha$. It is defined as the ratio of the perpendicular (spatial) mass of $\gamma_5$ to the parallel (temporal) mass: $\xi_f = M_\perp/M_\parallel$. This allows the tuning of the bare anisotropy $\xi_0$ appearing in the action.

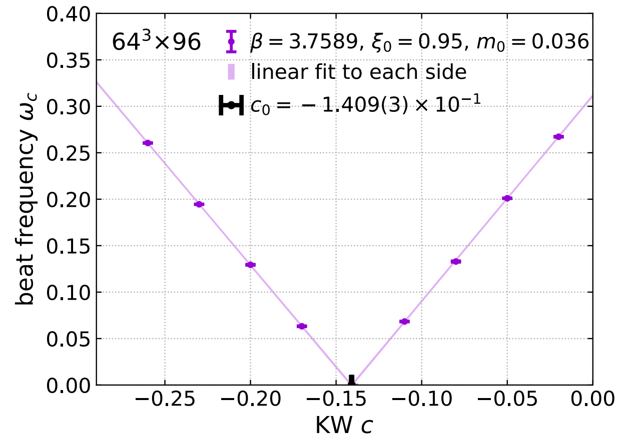


FIG. 5. The beat frequency $\omega_c$ as a function of the $c$ parameter. The $c$ parameter is tuned at the value where the beat frequency vanishes.

Following the procedure shown in Fig. 5, we tune $c$ for every value of $\xi_0$. Then, $\xi_0$ is tuned by imposing the desired renormalized anisotropy $\xi_f$. Since we perform measurements on isotropic staggered configurations, we tune by interpolating $\xi_f(\xi_0)$ at tuned $c$ to $\xi_f(\xi_0) = 1$. An example of this is shown in the top panel of Fig. 6.

At this point, it is necessary to simultaneously tune $c$ and $\xi_0$. Fortunately, the tuned value of $c$ depends only mildly on the tuned anisotropy $\xi_0$. Hence, with an interpolation of $c(\xi_0)$ to the tuned value $\xi_0$, we determine the final tuned $c, \xi_0$ pair (at fixed $m_0$). The bottom panel of Fig. 6 shows an example of this interpolation. In the top panel of Fig. 6 we also show with a black point the renormalized anisotropy $\xi_f$ from a dedicated run at the final tuned values of $c$ and $\xi_0$, which shows a result compatible with 1, hence confirming the validity of our procedure.

Finally, it is reasonable to ask how accurately one needs to tune $c$ and $\xi_0$, or how stable the result is to slight mistunings. Thankfully, the results are quite stable, as the $\xi_f(c)$ function has vanishing derivative (a maximum) near the tuned value. This is shown in Fig. 7.

This is not surprising: the anisotropy parameter does not break $C$ or $T$; i.e., it is even in $\zeta$, while a detuning of $c$ introduces an odd effect in $\zeta$. Thus, $d\xi/dc$ is odd and is expected to vanish up to higher orders in the lattice spacing, if the counterterm is correctly tuned. A similar behavior is observed with the mass of the pseudoscalar.

#### 3. *Tuning the bare mass $m_0$*

In this work, we carry out the tuning procedure first at a value of the pseudoscalar mass $M_{\gamma_5} = 578.4$ MeV. The final results of the tuning of $c$ and $\xi_0$ at several lattice spacings, with the $\gamma_5$ mass held constant at this value, are listed in Tables II and III. Then, we study the dependence of the tuned $c$ and $\xi_0$ values on $M_{\gamma_5}$, down to the physical pion mass. We find that the tuned value of $c$ for a given $\xi_0$ is very stable with respect to changes in $M_{\gamma_5}$. Moreover, for fixed $c$

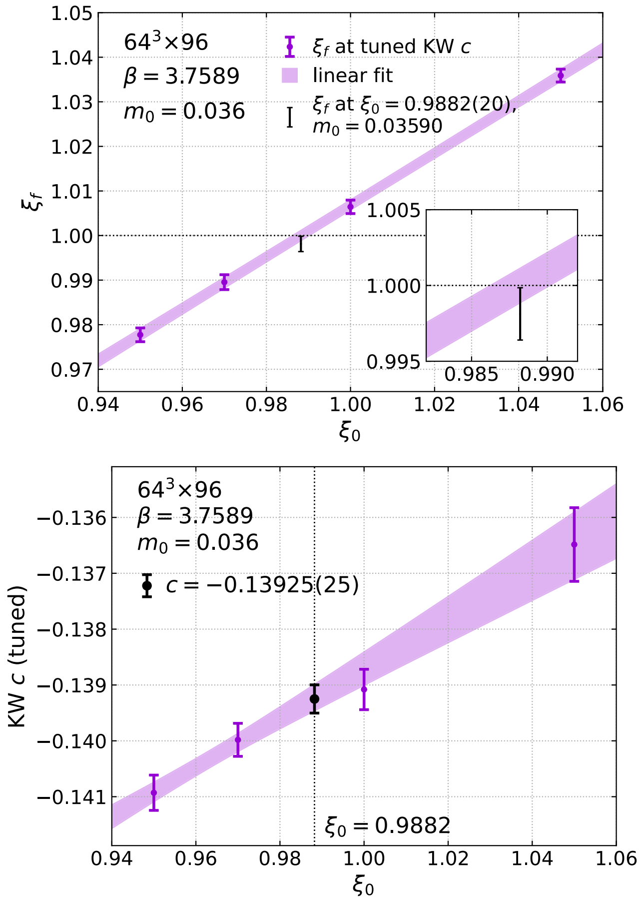


FIG. 6. Top: the renormalized fermion anisotropy $\xi_f = M_\perp/M_\parallel$ as a function of the bare anisotropy $\xi_0$. The $c$ parameter is individually tuned at each $\xi_0$ value. The tuning criterion for $\xi_0$ is $\xi_f = 1$. Bottom: interpolation to the tuned value of the $c$ parameter at the tuned value of $\xi_0$.

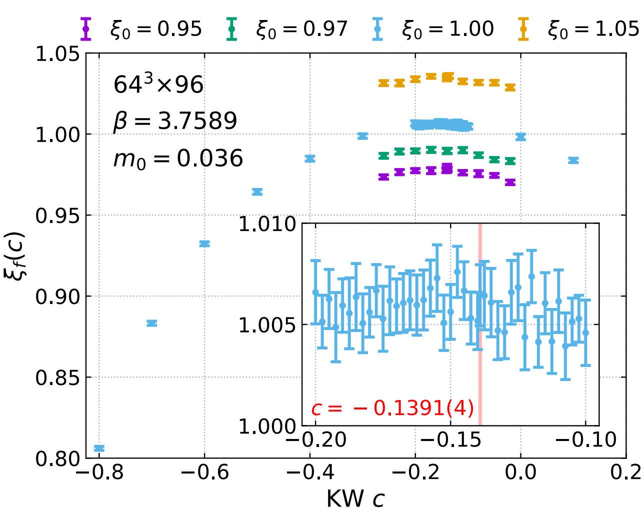


FIG. 7. The renormalized anisotropy $\xi_f$ as a function of the $c$ parameter at various fixed bare anisotropy values $\xi_0$. $\xi_f$ reaches a maximum around tuned $c$, and therefore it is stable against slight mistunings of $c$.

TABLE II. The tuned values of $c$, $\xi_0$ and $m_0$ for the unimproved action on the lattices used in this work. The bare mass $m_0$ is tuned to obtain $M_{\gamma_5} = 578.4$ MeV.

| $\beta$ | $a$ [fm] | $c$ | $\xi_0$ | $am_0$ |
|---|---|---|---|---|
| 3.6736 | 0.1581 | −0.18797 | 0.9943 | 0.05074 |
| 3.7089 | 0.1308 | −0.15733 | 0.9888 | 0.04131 |
| 3.7589 | 0.1152 | −0.13925 | 0.9882 | 0.03590 |
| 3.8360 | 0.0953 | −0.11703 | 0.9846 | 0.02937 |
| 4.0126 | 0.0638 | −0.08417 | 0.9854 | 0.01896 |

TABLE III. The tuned values of $c$, $\xi_0$ and $m_0$ for the Naik improved action on the lattices used in this work. The bare mass $m_0$ is tuned to obtain $M_{\gamma_5} = 578.4$ MeV.

| $\beta$ | $a$ [fm] | $c$ | $\xi_0$ | $am_0$ |
|---|---|---|---|---|
| 3.6736 | 0.1581 | −0.09387 | 1.12846 | 0.06102 |
| 3.7089 | 0.1308 | −0.07137 | 1.10280 | 0.04864 |
| 3.7589 | 0.1152 | −0.06129 | 1.09496 | 0.04205 |
| 3.8360 | 0.0953 | −0.04605 | 1.07397 | 0.03373 |

and $\xi_0$, the renormalized fermionic anisotropy $\xi_f$ is also very stable with respect to changes in $M_{\gamma_5}$, as its value remains in statistical agreement with 1 all the way down to the physical pion mass $M_{\gamma_5} = M_\pi \approx 135$ MeV. These results are shown in Fig. 8. Finally, $M_{\gamma_0}$ and $M_{\gamma_5}$ are concave functions of $c$, with a minimum near the tuned value of $c$. They are thus generally quite robust against mistunings of $c$, especially $M_{\gamma_5}$. Additional details on the dependence of $M_{\gamma_0}$ and $M_{\gamma_5}$ on $c$ can be found in Ref. [47].

### 4. Smearing

Lastly, we consider the effect of different levels of stout smearing on the tuning. In principle, each bare parameter has to be retuned at a new choice of the smearing level. We observe in the top panel of Fig. 9 that the actual pseudoscalar mass ($M_{\gamma_5}$) is within error independent on the smearing level while keeping the bare mass $m_0$ fixed. This allows us the simplification to address the variation of the counterterm $c$ with smearing using the same fixed $m_0$ value. For also a fixed value of $\xi_0$, we find the effect of applying more smearing steps to be a power law decrease in the magnitude of the tuned $c$ value. An example of this is shown in the bottom panel of Fig. 9.

Throughout this study, we will use four steps of stout smearing, the same smearing level that was used in the staggered simulations to generate the ensembles.

### 5. Hierarchy

To summarize, our tuning procedure proceeds in the following steps:

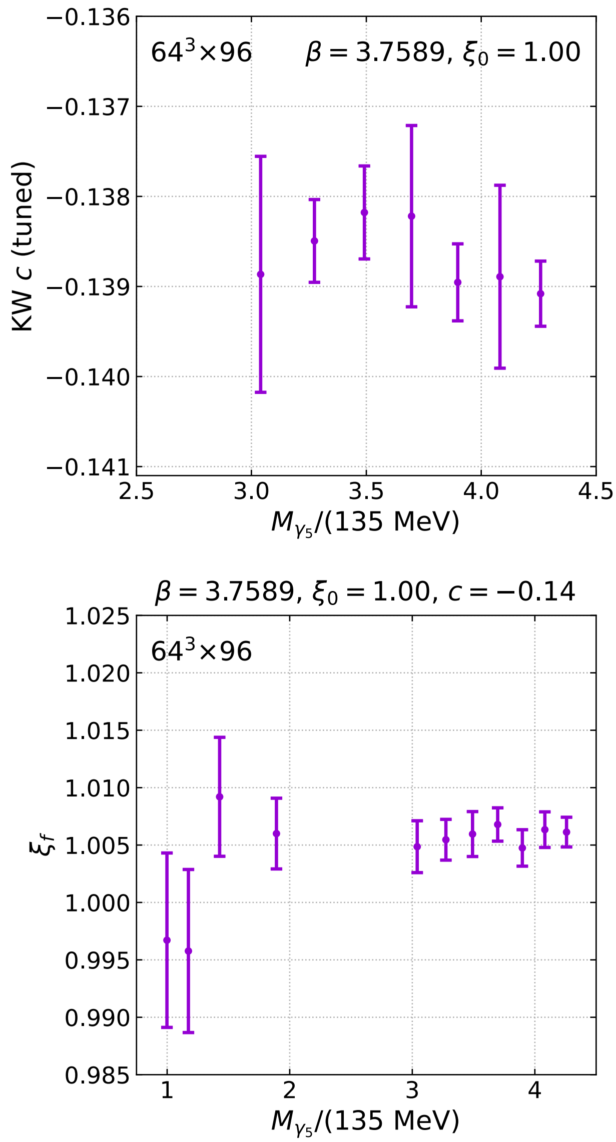


FIG. 8. Stability of the tuned $c$ value at fixed $\xi_0$ (top) and the renormalized anisotropy $\xi_f$ at fixed $\xi_0$ and $c$ (bottom) with respect to the pseudoscalar mass $M_{\gamma_5}$. $\xi_f$ remains stable even all the way down to the physical pion mass $M_\pi \approx 135$ MeV. The larger error bars at the small $M_{\gamma_5}$ values are due to smaller statistics.

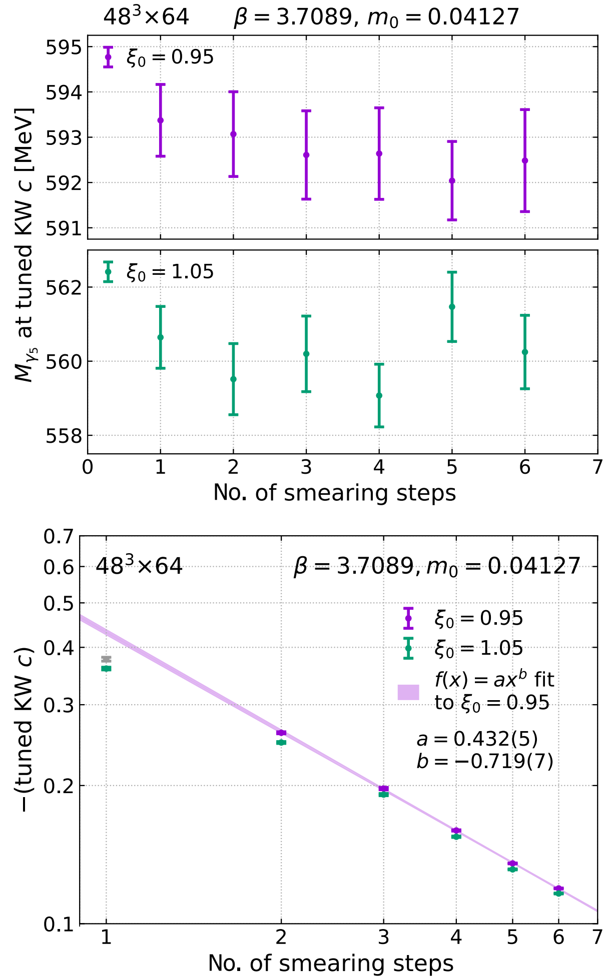


FIG. 9. Top: the pseudoscalar mass $M_{\gamma_5}$ as a function of the number of applied smearing steps. The number of smearing steps does not visibly affect the observed value of the mass. Bottom: the variation of the tuned value of $c$ for the case of the unimproved action with the number of stout smearing steps applied. We used four stout smearing steps throughout the rest of the analysis.

(1) tune $c$ at fixed bare anisotropy $\xi_0$, for a given pseudoscalar mass $M_{\gamma_5}$, which can be chosen to be large for numerical convenience;
(2) repeat the procedure for different $\xi_0$ values, tuning $c$ each time, then interpolate to $\xi_f(\xi_0) = 1$;
(3) interpolate the tuned $c$ at the tuned $\xi_0$;
(4) finally, tune the bare mass $m_0$ to fix the physical pseudoscalar mass ($c$ and $\xi_0$ do not need to be tuned again).

A hierarchy of the bare parameters is thus established. Most critical in the tuning procedure is the $c$ parameter, as the physical masses of oscillating fermion channels are highly dependent on it. The bare anisotropy $\xi_0$ follows in importance. Finally, the bare mass $m_0$ (alternatively the physical mass $M_{\gamma_5}$) is last, as it has the mildest effect.

## V. PION DECAY CONSTANT

In order to test both the unimproved and the Naik improved versions of our KW action, we turn to the computation of the pion decay constant $f_\pi$, which we extrapolate to the continuum in both cases. We also compare these results with staggered results on the same gauge ensembles, for which the quark mass was tuned to obtain the same value of $M_{\gamma_5} = 578.4$ MeV. Both KW actions are run with the parameters listed in Tables II and III. The three-hop action was not evaluated on the finest lattice due to memory limitations in the current implementation.

The pseudoscalar decay constant $f_\pi$ in the continuum (with the convention that the physical value is 131.5 MeV) is defined as

$$\langle \pi(p)|A_\mu(x)|0\rangle = e^{ipx} p_\mu f_\pi, \tag{23}$$

with the continuum partially conserved axial-vector current

$$A_\mu(x) = \bar{\psi}_u(x)\gamma_\mu\gamma_5\psi_d(x). \tag{24}$$

The corresponding Ward identity is

$$\partial_\mu A_\mu(x) = (m_u + m_d)P(x), \tag{25}$$

$$P(x) \equiv \bar{\psi}_u(x)\gamma_5\psi_d(x), \tag{26}$$

where $P(x)$ is the pseudoscalar density and $m_u$ and $m_d$ are the masses of quark $u$ and $d$, respectively. Therefore,

$$\frac{1}{\sqrt{V_{3d}}}\int_{\vec{x}} \langle \pi(m_\pi,\vec{0})|P(0,\vec{x})|0\rangle = \frac{1}{m_u+m_d} m_\pi^2 f_\pi, \tag{27}$$

where $m_\pi$ is the pion mass and $V_{3d}$ is the spatial 3-volume. On the lattice, the matrix element is renormalized as

$$\frac{1}{\sqrt{V_{3d}}}\sum_{\vec{x}} \langle \pi(m_\pi,\vec{0})|P(0,\vec{x})|0\rangle = \frac{Z_S}{Z_P}\frac{1}{m_u+m_d} m_\pi^2 f_\pi, \tag{28}$$

where $Z_S$ and $Z_P$ are the renormalization constants of scalar and pseudoscalar densities, respectively. Since all of staggered, unimproved and improved KW actions are chiral, $Z_S/Z_P = 1$. The pion correlator on the lattice between time slices $x_0$ and $y_0$, $G_{PP}(x_0, y_0)$, is defined as

$$G_{PP}(x_0,y_0) \equiv \frac{1}{V_{3d}}\sum_{\vec{x}}\sum_{\vec{y}} \langle 0|\bar{P}(x)P(y)|0\rangle. \tag{29}$$

Defining $\tau \equiv x_0 - y_0$, averaging over $y_0$, and using spectral decomposition, $\langle G_{PP}(y_0+\tau, y_0)\rangle_{y_0}$ acquires the following asymptotic form as $\tau \to \infty$:

$$\begin{aligned}
&\langle G_{PP}(y_0+\tau,y_0)\rangle_{y_0} \\
&\xrightarrow{\tau\to\infty} \left|\frac{1}{\sqrt{V_{3d}}}\sum_{\vec{x}}\langle \pi(m_\pi,\vec{0})|P(0,\vec{x})|0\rangle\right|^2 \frac{1}{2m_\pi} e^{-m_\pi\tau} \\
&= \left|\frac{Z_S}{Z_P}\frac{1}{m_u+m_d} m_\pi^2 f_\pi\right|^2 \frac{1}{2m_\pi} e^{-m_\pi\tau} \\
&= \frac{1}{2(m_u+m_d)^2} m_\pi^3 f_\pi^2 e^{-m_\pi\tau}.
\end{aligned} \tag{30}$$

In our simulation, the correlator is obtained stochastically by

$$\begin{aligned}
&C(\tau) \\
&\equiv C_0 \sum_{\vec{x},\vec{y},\vec{y}'} \langle \gamma_5 D^{-1}[U](y,x)\gamma_5 D^{-1}[U](x,y')\eta(y')\eta^\dagger(y)\rangle_{y_0,\eta,U},
\end{aligned} \tag{31}$$

where $x \equiv (y_0+\tau, \vec{x})$ and the Gaussian noise vectors $\eta$ are restricted on time slice $y_0$ [i.e., $y' = (y_0, \vec{y}')$] and satisfy

$$\langle \eta_{\alpha,a}(x)\eta^*_{\alpha',a'}(x')\rangle_\eta = \delta_{\alpha,\alpha'}\delta_{a,a'}\delta_{xx'} \tag{32}$$

with $\alpha, \alpha'$ and $a$, $a'$ being the spin and color indices, respectively. In this work, 16 $y_0$ time slices are separated evenly across the temporal extent of the lattice and one noise vector per time slice is used. The normalization constant $C_0$ is defined for staggered and KW actions, respectively, as

$$C_0^{\mathrm{Staggered}} \equiv \frac{1}{2}\frac{(m_u+m_d)^2}{V_{3d}}, \tag{33}$$

$$C_0^{\mathrm{KW}} \equiv \frac{(m_u+m_d)^2}{V_{3d}} \tag{34}$$

so that

$$C(\tau) \equiv 2(m_u+m_d)^2\langle G_{PP}(y_0+\tau, y_0)\rangle_{y_0}. \tag{35}$$

Hence $f_\pi$ and $m_\pi$ are readily obtained by the simple exponential form

$$C(\tau) \xrightarrow{\tau\to\infty} m_\pi^3 f_\pi^2 e^{-m_\pi\tau}. \tag{36}$$

In Fig. 10 we show the continuum extrapolation of $f_\pi$ measured using both the KW actions, as well as the

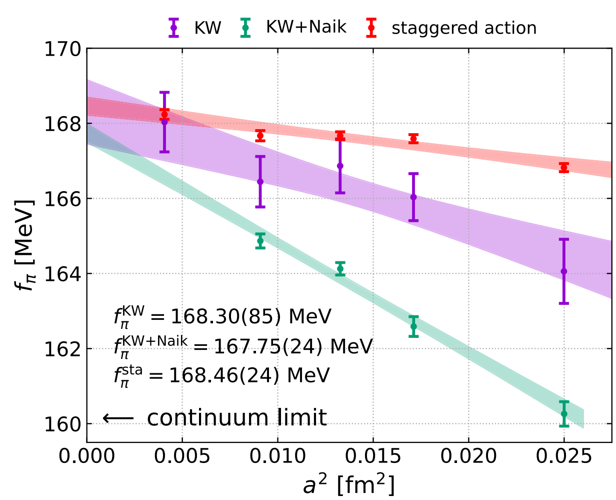


FIG. 10. Continuum extrapolation of the pion decay constant $f_\pi$ for the improved and unimproved KW action, as well as with the staggered action.

staggered one. All measurements used the same 144 configurations. In all three cases the points shown are the results of a systematic analysis of the uncertainties, where we varied the range of the fit and then combined the results with the histogram method [48]. The same treatment was used to estimate the uncertainties in Fig. 11. We find that the continuum limit of the unimproved KW action, due to its larger uncertainty, agrees with both the Naik improved KW action and the staggered one. With our current results, a slight tension appears between the Naik improved and staggered continuum limits. We also note that, with the same statistics, the Naik improved action yields substantially less noisy results, compared to the unimproved one. Moreover, the continuum limit has a 3× smaller error than the unimproved one, even without the use of the finest lattice. This fact bodes well for the cost effectiveness of the Naik improvement in the KW action.

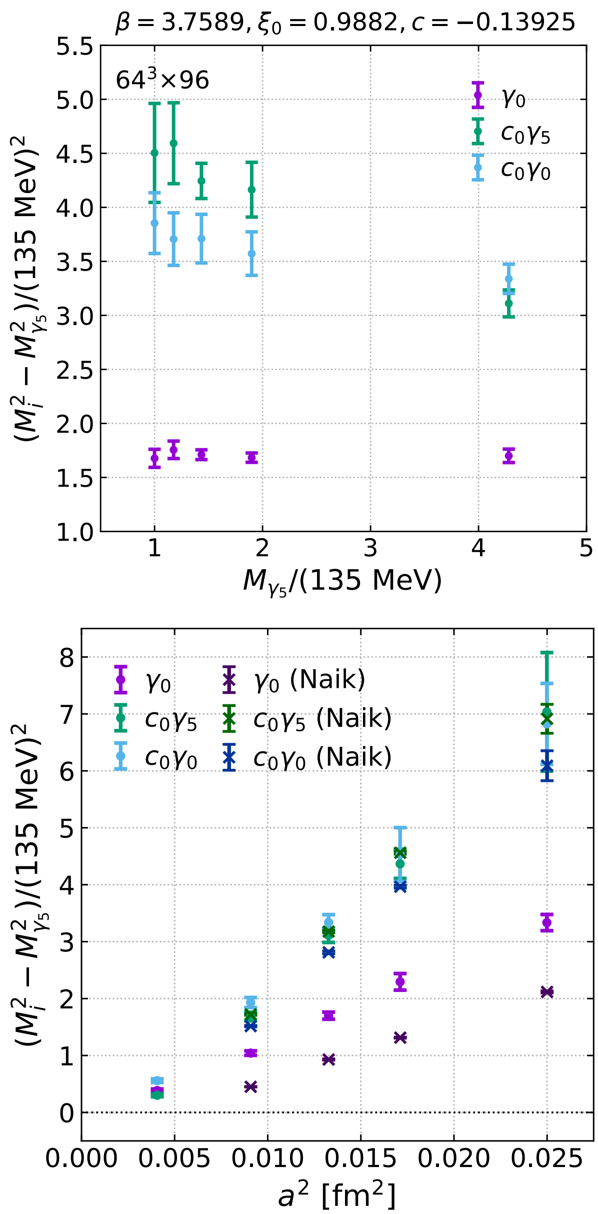


FIG. 11. Top: $M_{\gamma_5}$ dependence of the taste-splitting $\Delta M_i^2 = M_i^2 - M_{\gamma_5}^2$ of three fermion channels in the unimproved KW action with $\beta = 3.7589$. The $\gamma_0$ channel shows no $M_{\gamma_5}$ dependence even all the way down to the physical pion mass. The two site-split channels, $c_0\gamma_5$ and $c_0\gamma_0$, show a slight mass dependence, increasing as $M_{\gamma_5}$ decreases. Bottom: Taste splitting of the same three fermion channels on both the unimproved and Naik improved KW actions vs the lattice spacing squared at fixed $M_{\gamma_5} = 578.4$ MeV.

## VI. TASTE STRUCTURE

We now wish to gauge the impact of taste breaking in both the unimproved and Naik improved KW actions. Thus, we investigate the mass splittings of the ground states of various fermion channels that form parity partners in the spin-taste structure of the KW action [46]. For the naïve fermion action, the $\gamma_5$ and $\gamma_0$ channels are mass-degenerate parity partners, but they are no longer degenerate at finite lattice spacing for the KW action [30,46]. Reference [46] identifies "site-split" fermion operators $c_0\gamma_5$ and $c_0\gamma_0$ as parity partners in the same spin structure as $\gamma_5$ and $\gamma_0$.

We then consider the bare quark mass and lattice spacing dependence of the quadratic mass difference $\Delta M_i^2 = M_i^2 - M_{\gamma_5}^2$ for the three tastes $\gamma_0$, $c_0\gamma_5$, and $c_0\gamma_0$. We show in the top panel of Fig. 11 that $\Delta M_{\gamma_0}^2$ is very stable with respect to the pseudoscalar mass $M_{\gamma_5}$, even all the way down to the physical pion mass. This result agrees with the findings of Ref. [30]. For the $c_0\gamma_5$ and $c_0\gamma_0$ channels, the $M_{\gamma_5}$ dependence is small, although noticeable. The taste splitting of both channels increases as $M_{\gamma_5}$ decreases.

In the bottom panel of Fig. 11 we show $\Delta M_i^2$ at tuned $c$ and $\xi_0$ with $M_{\gamma_5} = 578.4$ MeV as a function of the lattice spacing squared for all three tastes. Results for both the unimproved and Naik improved action are shown. The rightmost points in the top panel are the (unimproved) middle points in the bottom plot. We find that $\Delta M_i^2$ decreases for $a \to 0$ for all three tastes. We find the effect of the improvement to be present mostly for the $\gamma_0$ channel, while the site-split channels are virtually unchanged. The $\gamma_0$ channel mass split is substantially reduced, from about 30% on the coarsest lattice to more than 50% on the finest simulated one. This is another argument in favor of the Naik improvement, which does seem to effectively reduce discretization errors and hence facilitate the continuum limit.

## VII. CONCLUSIONS

We have presented the results of a mixed-action study of the Karsten-Wilczek fermion action on 4stout staggered simulations, considering both an unimproved version and one with a tree-level Naik improvement in the three spatial directions. Although tedious, a tuning procedure involving the fixing of two fermionic counterterms, plus the bare quark mass, was formulated, whereby the different parameters might be tuned almost independently. A hierarchy in the tuning of the parameters was also established, based on the relative ease of the procedure, noting that the $c$ parameter should be fixed first, then the anisotropy $\xi_0$, and finally the quark mass. Importantly, this means that most of the tuning can be carried out at much cheaper, larger values of the mass, before being finalized at its physical value.

The investigation of the spatial Naik improvement showed that, with a reasonable cost increase, much less noisy results are obtained. The cost increase of a single iteration of the solver, compared to the unimproved case, is roughly a factor 2 (for the spatial part only). Additionally, as shown in Fig. 2 as a function of the inverse pseudoscalar mass, the number of iterations needed is also increased, by about 20%. The rightmost point in the plots roughly corresponds to a physical pion mass. In light of these additional costs, Fig. 10 can give us an idea of the comprehensive cost effectiveness of the Naik improvement. Overall, with an approximate per-lattice cost increase slightly above 2, we obtain roughly 4× smaller errors on the individual lattices. In the continuum extrapolation, the error reduction is of about a factor 3.5, even without simulating the finest lattice. Hence, we can conclude that the extra cost is more than compensated, and the Naik improved KW action should be used preferably.

Additionally, as we showed in our discussion of the taste-breaking features of the action, the improvement significantly reduces the mass split of the $\gamma_0$ channel, although the same does not happen for the site-split channels. It is also worth considering how the KW action compares to currently used actions, in particular staggered ones. In Fig. 12 we show the taste breaking of our 4stout and 4hex staggered actions, compared to our findings for the improved KW action, as a function of the lattice spacing. First, it is to be noted that the KW action has only four tastes, compared to the 16 of the staggered formulations. Shown in the plot are the squared-mass difference between a certain taste and the Goldstone (G) one, normalized by the squared physical pion mass. We show for the KW case the $\gamma_0$ channel (dashed line) and the root-mean-squared mass split (solid line). For the staggered actions, the dashed lines still indicate the second-lowest-lying state and solid lines the staggered tensor states. This is because these are the most numerous, and their mass is typically very close to the normalized mean square, for which they serve as good proxies.

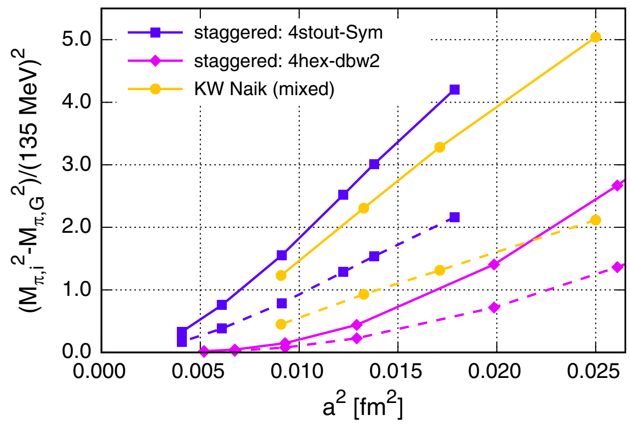


FIG. 12. Taste breaking in the KW action, compared to our 4stout and 4HEX staggered actions. The solid lines indicate the normalized mean-square taste breaking, while the dashed lines correspond to the second-lowest-lying states.

We find that both the normalized-mean-squared mass split and the lowest-lying channel in the improved KW sit slightly below the corresponding ones for the 4stout action. We also recall that the gauge ensembles used in this mixed study were generated with the same 4stout action, so that the yellow and purple points only differ by the fermionic measurements. We leave the exploration of the use of a different gauge action, smearing and anisotropy for future work.

In light of the results shown in this work, we can conclude that the Naik improved KW action is a valid alternative to currently employed staggered formulations because of the lack of rooting (with $N_f = 2$), as well as reasonable cost effectiveness and a favorable taste-breaking structure.

## ACKNOWLEDGMENTS

This work was partly funded from the DFG under Project No. 496127839. This work is also supported by the MKW NRW under the funding code NW21-024-A. The authors gratefully acknowledge the Gauss Centre for Supercomputing e.V. for funding this project by providing computing time on the GCS Supercomputer Juwels-Booster at Juelich Supercomputer Centre and HAWK at HLRS Stuttgart.

## DATA AVAILABILITY

The data supporting this study's findings are available within the article.

[1] B. Sheikholeslami and R. Wohlert, Improved continuum limit lattice action for QCD with Wilson fermions, Nucl. Phys. **B259**, 572 (1985).
[2] S. Durr, Z. Fodor, J. Frison, C. Hoelbling, R. Hoffmann *et al.*, Ab-initio determination of light hadron masses, Science **322**, 1224 (2008).
[3] J. B. Kogut and L. Susskind, Hamiltonian formulation of Wilson's lattice gauge theories, Phys. Rev. D **11**, 395 (1975).
[4] S. R. Sharpe, Rooted staggered fermions: Good, bad or ugly? Proc. Sci. LAT2006 (**2006**) 022 [arXiv:hep-lat/0610094].
[5] M. Golterman, Y. Shamir, and B. Svetitsky, Breakdown of staggered fermions at nonzero chemical potential, Phys. Rev. D **74**, 071501 (2006).
[6] M. Creutz, Chiral anomalies and rooted staggered fermions, Phys. Lett. B **649**, 230 (2007).
[7] M. Giordano, K. Kapas, S. D. Katz, D. Nogradi, and A. Pasztor, Radius of convergence in lattice QCD at finite $\mu_B$ with rooted staggered fermions, Phys. Rev. D **101**, 074511 (2020).
[8] I. M. Barbour, S. E. Morrison, E. G. Klepfish, J. B. Kogut, and M.-P. Lombardo, Results on finite density QCD, Nucl. Phys. B, Proc. Suppl. **60**, 220 (1998).
[9] Z. Fodor and S. Katz, A new method to study lattice QCD at finite temperature and chemical potential, Phys. Lett. B **534**, 87 (2002).
[10] Z. Fodor and S. Katz, Lattice determination of the critical point of QCD at finite T and mu, J. High Energy Phys. 03 (2002) 014.
[11] Z. Fodor and S. Katz, Critical point of QCD at finite T and mu, lattice results for physical quark masses, J. High Energy Phys. 04 (2004) 050.
[12] P. de Forcrand, S. Kim, and T. Takaishi, QCD simulations at small chemical potential, Nucl. Phys. B, Proc. Suppl. **119**, 541 (2003).
[13] A. Alexandru, M. Faber, I. Horvath, and K.-F. Liu, Lattice QCD at finite density via a new canonical approach, Phys. Rev. D **72**, 114513 (2005).
[14] Z. Fodor, S. D. Katz, and C. Schmidt, The density of states method at non-zero chemical potential, J. High Energy Phys. 03 (2007) 121.
[15] G. Endrodi, Z. Fodor, S. D. Katz, D. Sexty, K. K. Szabo, and C. Torok, Applying constrained simulations for low temperature lattice QCD at finite baryon chemical potential, Phys. Rev. D **98**, 074508 (2018).
[16] M. Giordano, K. Kapas, S. D. Katz, D. Nogradi, and A. Pasztor, Effect of stout smearing on the phase diagram from multiparameter reweighting in lattice QCD, Phys. Rev. D **102**, 034503 (2020).
[17] M. Giordano, K. Kapas, S. D. Katz, D. Nogradi, and A. Pasztor, New approach to lattice QCD at finite density; results for the critical end point on coarse lattices, J. High Energy Phys. 05 (2020) 088.
[18] S. Borsanyi, Z. Fodor, M. Giordano, S. D. Katz, D. Nogradi, A. Pasztor, and C. H. Wong, Lattice simulations of the QCD chiral transition at real baryon density, Phys. Rev. D **105**, L051506 (2022).
[19] S. Borsanyi, Z. Fodor, M. Giordano, J. N. Guenther, S. D. Katz, A. Pasztor, and C. H. Wong, Equation of state of a hot-and-dense quark gluon plasma: Lattice simulations at real μB vs extrapolations, Phys. Rev. D **107**, L091503 (2023).
[20] S. Borsanyi, Z. Fodor, M. Giordano, J. N. Guenther, S. D. Katz, A. Pasztor, and C. H. Wong, Can rooted staggered fermions describe nonzero baryon density at low temperatures?, Phys. Rev. D **109**, 054509 (2024).
[21] H. B. Nielsen and M. Ninomiya, No go theorem for regularizing chiral fermions, Phys. Lett. **105B**, 219 (1981).
[22] L. H. Karsten, Lattice fermions in euclidean space-time, Phys. Lett. **104B**, 315 (1981).
[23] F. Wilczek, On lattice fermions, Phys. Rev. Lett. **59**, 2397 (1987).
[24] M. Creutz, Four-dimensional graphene and chiral fermions, J. High Energy Phys. 04 (2008) 017.
[25] A. Borici, Creutz fermions on an orthogonal lattice, Phys. Rev. D **78**, 074504 (2008).
[26] S. Capitani, Reducing the number of counterterms with new minimally doubled actions, Phys. Rev. D **89**, 014501 (2014).
[27] S. Capitani, New actions for minimally doubled fermions and their counterterms, Proc. Sci., LATTICE2013 (**2014**) 121 [arXiv:1308.4512].
[28] S. Capitani, New chiral lattice actions of the Boriçi-Creutz type, Phys. Rev. D **89**, 074508 (2014).
[29] J. H. Weber, Correlation functions with Karsten-Wilczek fermions, Proc. Sci. LATTICE2014 (**2015**) 071 [arXiv:1601.06669].
[30] J. H. Weber, Properties of minimally doubled fermions, Ph.D. thesis, Mainz University, 2015, arXiv:1706.07104.
[31] G. Heatlie, G. Martinelli, C. Pittori, G. C. Rossi, and C. T. Sachrajda, The improvement of hadronic matrix elements in lattice QCD, Nucl. Phys. **B352**, 266 (1991).
[32] S. Borsanyi and S. Capitani, One-loop improved minimally doubled quarks (to be published).
[33] M. Creutz, T. Kimura, and T. Misumi, Index theorem and overlap formalism with naive and minimally doubled fermions, J. High Energy Phys. 12 (2010) 041.
[34] S. Dürr and J. H. Weber, Topological properties of minimally doubled fermions in two spacetime dimensions, Phys. Rev. D **105**, 114511 (2022).
[35] M. Pernici, Chiral invariance and lattice fermions with minimal doubling, Phys. Lett. B **346**, 99 (1995).
[36] P. F. Bedaque, M. I. Buchoff, B. C. Tiburzi, and A. Walker-Loud, Broken symmetries from minimally doubled fermions, Phys. Lett. B **662**, 449 (2008).
[37] S. Capitani, M. Creutz, J. Weber, and H. Wittig, Renormalization of minimally doubled fermions, J. High Energy Phys. 09 (2010) 027.
[38] H. W. Hamber and C. M. Wu, Some predictions for an improved fermion action on the lattice, Phys. Lett. **133B**, 351 (1983).
[39] S. Naik, On-shell improved lattice action for QCD with susskind fermions and asymptotic freedom scale, Nucl. Phys. **B316**, 238 (1989).
[40] E. Follana *et al.* (HPQCD and UKQCD Collaborations), Highly improved staggered quarks on the lattice, with applications to charm physics, Phys. Rev. D **75**, 054502 (2007).
[41] R. Bellwied, S. Borsanyi, Z. Fodor, S. D. Katz, A. Pasztor, C. Ratti, and K. K. Szabo, Fluctuations and correlations in high temperature QCD, Phys. Rev. D **92**, 114505 (2015).
[42] S. Borsanyi *et al.*, High precision scale setting on the lattice, Proc. Sci. LATTICE2021 (**2022**) 371.

[43] M. Luscher, Computational strategies in lattice QCD, in *Les Houches Summer School: Session 93: Modern Perspectives in lattice QCD: Quantum Field Theory and High Performance Computing* (2010), pp. 331–399, arXiv:1002.4232.

[44] Y. Saad, *Iterative Methods for Sparse Linear Systems* (Society for Industrial and Applied Mathematics, 2003), 10.1137/1.9780898718003.

[45] J. H. Weber, QCD with flavored minimally doubled fermions, Proc. Sci. LATTICE2016 (**2017**) 250 [arXiv: 1611.08388].

[46] J. H. Weber, Spin-taste structure of minimally doubled fermions, Proc. Sci. LATTICE2023 (**2024**) 353 [arXiv: 2312.08526].

[47] D. A. Godzieba, S. Borsanyi, Z. Fodor, P. Parotto, R. A. Vig, and C. H. Wong, Renormalization of Karsten-Wilczek quarks on a staggered background, Proc. Sci. LATTICE2023 (**2024**) 283 [arXiv:2401.07799].

[48] S. Borsanyi *et al.*, Leading hadronic contribution to the muon magnetic moment from lattice QCD, Nature (London) **593**, 51 (2021).